

# Dynamics of charge imbalance resolved entanglement negativity after a local joining quench

Hui-Huang Chen<sup>a\*</sup>, Zun-Xian Huang<sup>a†</sup>

August 8, 2023

<sup>a</sup>*College of Physics and Communication Electronics, Jiangxi Normal University, Nanchang 330022, China*

## Abstract

In this paper, we consider the dynamics of charge imbalance resolved negativity after a local joining quench. We first study the local joining quench by applying the CFT approach. We calculate the quench dynamics of charged logarithmic negativity. By using the Fourier transformation, we obtain the charge imbalance resolved negativity. Then the total negativity can be recovered from the charged imbalance resolved ones. We test our CFT predictions in the lattice model numerically. Finally, we explain our results based on the quasi-particle picture.

---

\*chenhh@jxnu.edu.cn

†202140100617@jxnu.edu.cn

# Contents

<b>1</b>	<b>Introduction</b>	<b>2</b>
<b>2</b>	<b>Local joining quench</b>	<b>3</b>
<b>3</b>	<b>Charge logarithmic negativity and charge imbalance resolved negativity</b>	<b>4</b>
3.1	Charge logarithmic negativity . . . . .	4
3.2	Charge imbalance resolved negativity . . . . .	6
<b>4</b>	<b>Evolution of charged logarithmic negativity in local joining quench</b>	<b>7</b>
4.1	Two adjacent intervals . . . . .	7
4.1.1	Semi-infinite intervals . . . . .	7
4.1.2	Symmetric finite intervals . . . . .	9
4.1.3	Asymmetric finite intervals . . . . .	9
4.2	Two disjoint intervals . . . . .	10
4.2.1	Symmetric finite intervals . . . . .	10
4.2.2	Asymmetric finite intervals . . . . .	10
<b>5</b>	<b>Charge imbalance resolved negativity in local joining quench</b>	<b>11</b>
5.1	Two adjacent intervals . . . . .	11
5.1.1	Semi-infinite intervals . . . . .	11
5.1.2	Symmetric finite intervals . . . . .	11
5.2	Two disjoint symmetric finite intervals . . . . .	12
5.3	Total negativity . . . . .	13
<b>6</b>	<b>Numerical test</b>	<b>13</b>
6.1	Numerical approach . . . . .	13
6.2	Comparison between CFT predictions and numerical results . . . . .	18
<b>7</b>	<b>Conclusion</b>	<b>19</b>

# 1 Introduction

Over the last two decades, various entanglement measures have played crucial roles in relating diverse fields ranging from field theories and many-body physics to quantum gravity and black hole physics [1–7]. In field theories and many-body physics, entanglement is used for characterizing different phase of matter. In quantum gravity and black hole physics, since Ryu and Takayanagi first proposed the notion of holographic entanglement entropy [8], a large number of studies have emerged, including holographic entanglement entropy [9–13], holographic entanglement negativity [14–18].

Among the aforesaid research progresses, entanglement entropy is the most successful entanglement measure to characterize the bipartite entanglement of a subsystem  $A$  in a pure state. Given a system in a pure state, the reduced density matrix (RDM) of a subsystem  $A$  is defined by tracing out its complement  $B$  as  $\rho_A = \text{Tr}_B |\Psi\rangle\langle\Psi|$ , the Rényi entropies are defined as

$$S_n = \frac{1}{1-n} \log \text{Tr} \rho_A^n, \quad (1.1)$$

then we can obtain the Von Neumann entropy through the replica trick [1]

$$S_1 \equiv \lim_{n \rightarrow 1} S_n = - \lim_{n \rightarrow 1} \frac{\partial}{\partial n} \text{Tr} \rho_A^n = -\text{Tr}(\rho_A \log \rho_A). \quad (1.2)$$

When two subsystems  $A_1$  and  $A_2$  embedded in a larger system are not necessarily complementary to each other,  $\rho_{A_1 \cup A_2}$  is general a mixed state. Entanglement entropy is no longer a good measure of entanglement, since it mixes classical and quantum correlations. A computable measure of the bipartite entanglement for a general mixed state, entanglement negativity can be defined as [19]

$$\mathcal{N} = \frac{\text{Tr} |\rho_A^{T_2}| - 1}{2}, \quad (1.3)$$

where  $\text{Tr}|O| = \text{Tr}\sqrt{O^\dagger O}$  denotes the trace norm of the operator  $O$  and  $\rho_A^{T_2}$  is partial transpose of RDM  $\rho_A$  with respect to the degree of freedom of subsystem  $A_2$ . In detail, given the bases  $|e_i^1\rangle$  and  $|e_j^2\rangle$  of the respective Hilbert spaces  $\mathcal{H}_1$  and  $\mathcal{H}_2$ , the partial transposition with respect to the degrees of freedom of subsystem  $A_2$  is defined as

$$\langle e_i^{(1)} e_j^{(2)} | \rho_A^{T_2} | e_k^{(1)} e_l^{(2)} \rangle = \langle e_i^{(1)} e_l^{(2)} | \rho_A | e_k^{(1)} e_j^{(2)} \rangle. \quad (1.4)$$

The Rényi negativity and Rényi logarithmic negativity are defined as

$$\mathcal{N}_n = \frac{N_n - 1}{2}, \quad \mathcal{E}_n = \log N_n, \quad N_n = \text{Tr}[(\rho_A^{T_2})^n], \quad (1.5)$$

from which the negativity and logarithmic negativity are obtained by using the analytic continuation of the even integer at  $n_e = 1$

$$\mathcal{N} = \lim_{n_e \rightarrow 1} \mathcal{N}_{n_e}, \quad \mathcal{E} = \lim_{n_e \rightarrow 1} \mathcal{E}_{n_e}. \quad (1.6)$$

Recently the non-equilibrium evolution of isolated quantum system is one of the most active research areas. The most studied situation is quantum quench [20]. Entanglement negativity following a quantum quench has been studied in field theories [21, 22] and holographic theories [23, 24]. In the context of a quantum quench, an interesting question concerns the interplay

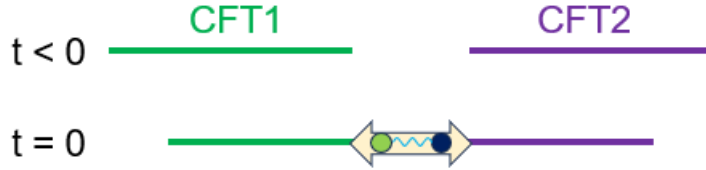


Figure 1: Setup for local joining quench. Two separate CFTs are joined together at their endpoints at time  $t = 0$ . Entangled pairs which carry entanglement information are quasi-particles generated at the joining point propagating through the system.

between symmetries and entanglement [25, 26]. When a system has a global symmetry, the entanglement entropy and negativity will split into different symmetry sectors characterized by eigenvalues of some charge operator. The concept of symmetry-resolved entanglement particularly attracted much attention in both condensed matter physics [27–31] and holographic theories [32].

The dynamics of charge imbalance resolved negativity after a global quench in the free Fermion and Bose model was investigated in [33] and [34]. In Ref. [35], the dynamics of charge resolved entropy and negativity after a local quench was studied in the XXZ model and XX model. Although many works have been done on the symmetry-resolved entanglement negativity after a quantum quench, there is a gap in the time evolution of the charged negativity and imbalance entanglement negativity after local joining quench. In this paper, we will fill this gap by studying the dynamics of the charged logarithmic negativity and imbalance entanglement negativity after local joining quench for two adjacent and disjoint intervals cases.

Following the method in Refs. [21, 22], as shown in Fig.1, here we consider a local joining quench in a (1+1)-dimensional critical system, which is physically cut into two parts prepared in their own ground states at time  $t < 0$ . We join the two parts together at their endpoints at time  $t = 0$ , then they evolve together. At the same time, the interaction between them is produced and quasi-particles (which can be viewed as entangle pairs [36]) are generated at the joining point.

The plan of this paper is as follows. In section 2, we briefly introduce the CFT setup for local joining quench. In section 3, we review how to compute the time evolution of charged logarithmic negativity and charged imbalance resolved negativity after local joining quench. In section 4, we consider the time evolution of charged logarithmic negativity between two adjacent and disjoint intervals in the local joining quench protocol. In section 5, we will calculate the charge imbalance resolved negativity from the results obtained in the previous sections. In section 6, we compare our CFT predictions with the numerical results in the complex harmonic chain. We further explain our results for the charged logarithmic negativity based on the quasi-particle picture. Finally, in section 7, we conclude our results and discuss some interesting problems which are worth investigating in the future.

## 2 Local joining quench

In this section, we briefly review the CFT approach to the local joining quench following Ref. [37]. We first introduce the time evolution of the density matrix  $\rho(t) = |\phi(x, t)\rangle\langle\phi(x, t)|$

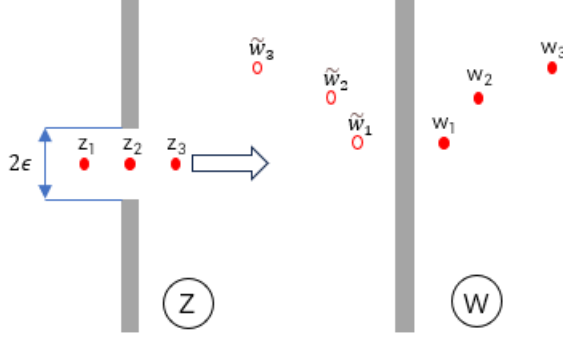


Figure 2: The conformal mapping in Eq.(2.2), based on which the  $z$ -plane is mapped to a right half plane (RHP) with  $\text{Re}(w) > 0$ .

with  $|\phi(x, t)\rangle = e^{-iHt}|\phi_0(x)\rangle$ . It has the following path integral representation

$$\langle \phi''(x'') | \rho(t) | \phi'(x') \rangle = Z^{-1} \langle \phi''(x'') | e^{-iHt - \epsilon H} | \phi_0(x) \rangle \langle \phi_0(x) | e^{+iHt - \epsilon H} | \phi'(x') \rangle, \quad (2.1)$$

where two factors  $e^{-\epsilon H}$  are used to make the path integral absolutely convergent and  $Z = \langle \phi_0 | e^{-2\epsilon H} | \phi_0 \rangle$  is the normalization factor. We can express the density matrix using the path integral on a modified world-sheet, as shown in Fig.2, where the physical cut corresponds to having a slit parallel to the imaginary time axis, giving two parts with one starting from  $-\infty$  up to  $\tau_1 = -\epsilon - it$  and the other starting from  $\tau_2 = +\epsilon - it$  to  $+\infty$  in the complex  $z$ -plane. For computation simplicity, we map the  $z$ -plane to a right half plane (RHP), with  $\text{Re}(w) > 0$  in terms of the conformal mapping

$$w(z) = \frac{z}{\epsilon} + \sqrt{\left(\frac{z}{\epsilon}\right)^2 + 1}, \quad z(w) = \epsilon \frac{w^2 - 1}{2w}. \quad (2.2)$$

Then the problem of local joining quench is reduced to the computation of the correlation functions of the fluxed twist fields in the RHP.

### 3 Charge logarithmic negativity and charge imbalance resolved negativity

As shown in Fig.3, we consider the cases of two semi-infinite intervals (up), two adjacent intervals (middle), and two disjoint intervals (bottom). In three cases, we will respectively calculate the dynamics of charged logarithmic negativity after local joining quench in CFT. we will review the computation of the charge logarithmic negativity and charge imbalance resolved negativity in this section.

#### 3.1 Charge logarithmic negativity

We will review some basic facts about the charged logarithmic negativity in  $(1+1)$  dimensional CFT (see [38] for more details). We assume that our system exhibits a global  $U(1)$  symmetry and the subsystem  $A$  consists of  $N$  disjoint intervals. It is convenient to introduce the charged moments of  $\rho_A$

$$Z_n(\mu) = \text{Tr}(\rho_A^n e^{i\mu Q_A}), \quad (3.1)$$

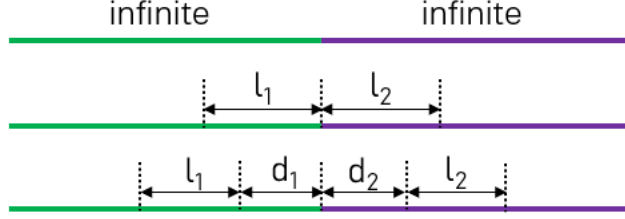


Figure 3: Different cases we consider here: semi-infinite intervals (up), two adjacent intervals (middle) and two disjoint intervals (bottom).

then we can view it as the partition function on the Riemann surface  $\mathcal{R}_{n,N}$  pierced by an Aharonov-Bohm flux, such that the total phase accumulated by the field upon going through the entire surface is  $\mu$ . We can define the operator  $\mathcal{V}_\mu$  and the local twist field  $\mathcal{T}_n$  which generate the total phase  $\mu$  and the  $n$ -sheet Riemann surface  $\mathcal{R}_{n,N}$ , respectively. We call the fusion of  $\mathcal{V}_\mu$  and  $\mathcal{T}_n$  as fluxed twist field denoted by  $\mathcal{T}_{n,\mu}$  [27]. Then the partition function on the fluxed Riemann surface  $\mathcal{R}_{n,N}^{(\mu)}$  is obtained from the  $2N$ -point function of these fluxed twist operators. The dimension of fluxed twist field and fluxed anti-twist fields have the same quantity, it reads [38]

$$\Delta_{n,\mu} = \frac{1}{6} \left( n - \frac{1}{n} \right) - \frac{\mu^2}{4\pi^2 n} + \frac{\mu}{2\pi n}. \quad (3.2)$$

For simplicity, in the following part, we will focus on the case  $N = 2$ , i.e. we will consider that the subsystem  $A$  is made of two disjoint intervals  $A_1 = [l_1, l_2]$  and  $A_2 = [l_3, l_4]$  on the real axis,  $A = A_1 \cup A_2$ . The charged moments of the partially transposed RDM is given by [38]

$$\text{Tr}[(\rho_A^{T_2})^n e^{i\mu \mathcal{Q}_A}] = \langle \mathcal{T}_{n,\mu}(z_1) \tilde{\mathcal{T}}_{n,\mu}(z_2) \tilde{\mathcal{T}}_{n,\mu}(z_3) \mathcal{T}_{n,\mu}(z_4) \rangle_{\text{strip}}, \quad z_i = l_i + i\tau, \quad (3.3)$$

where we have exchanged the fluxed twist field  $\mathcal{T}_{n,\mu}$  and  $\tilde{\mathcal{T}}_{n,\mu}$  at the endpoints of  $A_2$  while keep the others unchanged. By using the conformal mapping defined in Eq. (2.2), the four-point function on the strip is mapped onto the RHP, then we have

$$\text{Tr}[(\rho_A^{T_2})^n e^{i\mu \mathcal{Q}_A}] = \prod_{i=1}^4 \left| \frac{dw}{dz} \right|_{z_i}^{\Delta(i)} \left\langle \mathcal{T}_{n,\mu}(w_1) \tilde{\mathcal{T}}_{n,\mu}(w_2) \tilde{\mathcal{T}}_{n,\mu}(w_3) \mathcal{T}_{n,\mu}(w_4) \right\rangle_{\text{RHP}}, \quad (3.4)$$

where the scaling dimensions  $\Delta(1) = \Delta(2) = \Delta(3) = \Delta(4) = \Delta_{n,\mu}$ . In terms of global conformal symmetry, the four-point function on the RHP has the following form

$$\begin{aligned} & \left\langle \mathcal{T}_{n,\mu}(w_1) \tilde{\mathcal{T}}_{n,\mu}(w_2) \tilde{\mathcal{T}}_{n,\mu}(w_3) \mathcal{T}_{n,\mu}(w_4) \right\rangle_{\text{RHP}} \\ &= \frac{c_{n,\mu}^2}{\prod_{i=1}^4 |(w_i - \tilde{w}_i)/a|^{\Delta_{n,\mu}}} \frac{1}{\eta_{1,2}^{\Delta_{n,\mu}} \eta_{3,4}^{\Delta_{n,\mu}}} \left( \frac{\eta_{1,4} \eta_{2,3}}{\eta_{1,3} \eta_{2,4}} \right)^{\Delta_{n,\mu}^{(2)}/2 - \Delta_{n,\mu}} \mathcal{F}_n(\{\eta_{j,k}\}), \end{aligned} \quad (3.5)$$

where the constant  $c_{n,\mu}$  known for some specific theories are nonuniversal and  $a$  is an UV cutoff. The cross ratios  $\eta_{i,j} = \frac{(w_i - w_j)(\tilde{w}_i - \tilde{w}_j)}{(w_i - \tilde{w}_j)(\tilde{w}_i - w_j)}$  with  $\tilde{w}_i = -\bar{w}_i$ , which is the image of  $w_i$  as shown in Fig.2. The nonuniversal function  $\mathcal{F}_n(\{\eta_{j,k}\})$  depends on the full operator content of the theory and is very difficult to calculate.

When we take the limit  $z_3 \rightarrow z_2$ , the charged moments of the partially transposed RDM for two adjacent intervals has the simpler structure

$$\begin{aligned} \text{Tr}[(\rho_A^{T_2})^n e^{i\mu\mathcal{Q}_A}] &= \left\langle \mathcal{T}_{n,\mu}(z_1) \tilde{\mathcal{T}}_{n,\mu}^2(z_2) \mathcal{T}_{n,\mu}(z_3) \right\rangle_{\text{strip}} \\ &= \prod_{i=1}^3 \left| \frac{dw}{dz} \right|_{z_i}^{\Delta(i)} \left\langle \mathcal{T}_{n,\mu}(w_1) \tilde{\mathcal{T}}_{n,\mu}^2(w_2) \mathcal{T}_{n,\mu}(w_3) \right\rangle_{\text{RHP}}, \end{aligned} \quad (3.6)$$

where the scaling dimensions  $\Delta_{(1)} = \Delta_{(3)} = \Delta_{n,\mu}$  and  $\Delta_{(2)} = \Delta_{n,\mu}^{(2)}$ . Then the three-point function on the RHP has the standard form

$$\langle \mathcal{T}_{n,\mu}(w_1) \tilde{\mathcal{T}}_{n,\mu}^2(w_2) \mathcal{T}_{n,\mu}(w_3) \rangle_{\text{RHP}} = \frac{c_{n,\mu}}{\prod_{i=1}^3 |(w_i - \tilde{w}_i)/a|^{\Delta(i)}} \left( \frac{\eta_{1,3}^{\Delta_{n,\mu}^{(2)} - 2\Delta_{n,\mu}}}{\eta_{1,2}^{\Delta_{n,\mu}^{(2)}} \eta_{2,3}^{\Delta_{n,\mu}^{(2)}}} \right)^{1/2} \mathcal{F}_n(\{\eta_{j,k}\}). \quad (3.7)$$

The charged Rényi negativity is equivalent to the charged moments of the partially transposed RDM

$$N_n(\mu) = \text{Tr}[(\rho_A^{T_2})^n e^{i\mu\mathcal{Q}_A}], \quad (3.8)$$

the charged negativity is obtained by taking the replica limit  $n_e \rightarrow 1$

$$N(\mu) = \lim_{n_e \rightarrow 1} N_{n_e}(\mu), \quad (3.9)$$

the charged logarithmic negativity is given by

$$\mathcal{E}(\mu) = \log N(\mu). \quad (3.10)$$

### 3.2 Charge imbalance resolved negativity

We briefly recall some results about the charge imbalance resolved negativity under the U(1) symmetry generated by a local charge Q (see [28, 30, 33, 34] for more details). We consider the case of a bi-partition in two complementary subsystems  $A$  and  $B$ , in which the subsystem  $A$  is partitioned into two complementary subsystems  $A_1$  and  $A_2$ , we denote the corresponding charge operators as  $Q_1$  and  $Q_2$ . Because of locality, we can get  $Q = Q_A + Q_B$  and  $Q_A = Q_1 + Q_2$ . From the relation  $[\rho_A, Q_A] = 0$ , performing the partial transpose with respect to the degrees of freedom of subsystem  $A_2$ , we have

$$[\rho_A^{T_2}, \mathcal{Q}_A] = 0, \quad \mathcal{Q}_A = Q_1 - Q_2^{T_2}, \quad (3.11)$$

where we define the operator  $\mathcal{Q}_A$  as charge imbalance operator. We denote the eigenvalues of the charge imbalance operator  $\mathcal{Q}_A$  by  $q$ . We also denote the projectors on the corresponding eigenspace by  $\mathcal{P}_q$ , which has the following explicit form

$$\mathcal{P}_q = \int_0^{2\pi} \frac{d\mu}{2\pi} e^{-i\mu q} e^{i\mu\mathcal{Q}_A}. \quad (3.12)$$

Then  $\rho_A^{T_2}$  has a form of block matrix, each block is characterized by different eigenvalues  $q$ , thus we can write

$$\rho_A^{T_2}(q) = \frac{\mathcal{P}_q \rho_A^{T_2}}{\text{Tr}(\mathcal{P}_q \rho_A^{T_2})}. \quad (3.13)$$

It is enough to write

$$\rho_A^{T_2} = \oplus_{\mathbf{q}} p(\mathbf{q}) \rho_A^{T_2}(\mathbf{q}), \quad (3.14)$$

where  $p(\mathbf{q}) = \text{Tr}[\mathcal{P}_{\mathbf{q}} \rho_A^{T_2}]$  is the probability of finding  $\mathbf{q}$  as the outcome of a measurement of  $\mathcal{Q}_A$ . The charge imbalance resolved negativity is defined as

$$\mathcal{N}(\mathbf{q}) = \frac{\text{Tr}|\rho_A^{T_2}(\mathbf{q})| - 1}{2}, \quad \mathcal{N} = \sum_{\mathbf{q}} p(\mathbf{q}) \mathcal{N}(\mathbf{q}), \quad (3.15)$$

where  $\mathcal{N}$  is the total negativity obtained by the sum of charge imbalance resolved negativity weighted by the corresponding probability. It is useful to define the charge imbalance resolved Rényi negativity as

$$\mathcal{N}_n(\mathbf{q}) = \frac{N_n(\mathbf{q}) - 1}{2}, \quad N_n(\mathbf{q}) = \text{Tr}[(\rho_A^{T_2}(\mathbf{q}))^n] = \frac{\text{Tr}[\mathcal{P}_{\mathbf{q}}(\rho_A^{T_2})^n]}{p(\mathbf{q})^n}, \quad (3.16)$$

then we have the charged imbalance resolved negativity

$$\mathcal{N}(\mathbf{q}) = \lim_{n_e \rightarrow 1} \mathcal{N}_{n_e}(\mathbf{q}). \quad (3.17)$$

The charged Rényi negativity and its Fourier transformation are

$$N_n(\mu) = \text{Tr}[(\rho_A^{T_2})^n e^{i\mu \mathcal{Q}_A}], \quad \mathcal{Z}_{T_2, n}(\mathbf{q}) = \int_0^{2\pi} \frac{d\mu}{2\pi} e^{-i\mu \mathbf{q}} N_n(\mu), \quad (3.18)$$

for  $n = 1$ , we obtain the charged probability  $N_1(\mu)$ , since its Fourier transformation gives the probability

$$N_1(\mu) = \text{Tr}[\rho_A^{T_2} e^{i\mathcal{Q}_A \mu}], \quad p(\mathbf{q}) = \int_0^{2\pi} \frac{d\mu}{2\pi} e^{-i\mu \mathbf{q}} N_1(\mu) = \int_0^{2\pi} \frac{d\mu}{2\pi} e^{-i\mu \mathbf{q}} e^{\mathcal{E}_1(\mu)}, \quad (3.19)$$

then it is easy to drive

$$N_n(\mathbf{q}) = \frac{\mathcal{Z}_{T_2, n}(\mathbf{q})}{p(\mathbf{q})^n}. \quad (3.20)$$

We also introduce the quantity

$$\mathcal{Z}_{T_2}(\mathbf{q}) \equiv \lim_{n_e \rightarrow 1} \mathcal{Z}_{T_2, n_e}(\mathbf{q}) = \int_0^{2\pi} \frac{d\mu}{2\pi} e^{-i\mu \mathbf{q}} e^{\mathcal{E}(\mu)}, \quad (3.21)$$

from which we can obtain the charge imbalance resolved negativity

$$\mathcal{N}(\mathbf{q}) = \frac{1}{2} \left( \frac{\mathcal{Z}_{T_2}(\mathbf{q})}{p(\mathbf{q})} - 1 \right) = \frac{1}{2} \left( \frac{\int_0^{2\pi} \frac{d\mu}{2\pi} e^{-i\mu \mathbf{q}} e^{\mathcal{E}(\mu)}}{\int_0^{2\pi} \frac{d\mu}{2\pi} e^{-i\mu \mathbf{q}} e^{\mathcal{E}_1(\mu)}} - 1 \right). \quad (3.22)$$

## 4 Evolution of charged logarithmic negativity in local joining quench

### 4.1 Two adjacent intervals

#### 4.1.1 Semi-infinite intervals

As shown in Fig.3, it is convenient to consider the simplest case, in which the total system is made of two semi-infinite parts  $A_1$  and  $A_2$ . In this case, the time evolution of charged Rényi



negativity is governed by  $\langle \mathcal{T}_{n,\mu}^2(z_1) \rangle$  on the strip where  $\mathcal{T}_{n,\mu}^2(z_1)$  is a single fluxed twist field inserted at  $z_1 = l + i\tau$  in the  $z$ -plane. Here we choose  $l = 0$ , we get  $z_1 = i\tau$ . The expectation value of  $\mathcal{T}_{n,\mu}^2(z_1)$  has the standard form

$$\langle \mathcal{T}_{n,\mu}^2(z_1) \rangle = c_{n,\mu} \left( \left| \frac{dw}{dz} \right|_{z_1} \frac{a}{2 \operatorname{Re}(w_1)} \right)^{\Delta_{n,\mu}^{(2)}}, \quad (4.1)$$

where the scaling dimension  $\Delta_{n,\mu}^{(2)}$  of the fluxed twist field  $\mathcal{T}_{n,\mu}^2(z_1)$  reads [34]

$$\Delta_{n,\mu}^{(2)} = \begin{cases} \Delta_{n,2\mu}, & \text{odd } n \\ 2\Delta_{\frac{n}{2},\mu}, & \text{even } n \end{cases} \quad (4.2)$$

In terms of the conformal mapping in Eq. (2.2), we obtain

$$w_1 = i\frac{\tau}{\epsilon} + \frac{1}{\epsilon} \sqrt{\epsilon^2 - \tau^2}, \quad (4.3)$$

then we can get

$$\left| \frac{dw}{dz} \right|_{z_1} = \frac{1}{\sqrt{\epsilon^2 - \tau^2}}. \quad (4.4)$$

After considering the real  $\tau$  and only at the end of the computation using an analytical continuation  $\tau \rightarrow it$ , we find

$$\langle \mathcal{T}_{n,\mu}^2(z_1) \rangle = c_{n,\mu} \left( \frac{a\epsilon}{2(\epsilon^2 + t^2)} \right)^{\Delta_{n,\mu}^{(2)}}. \quad (4.5)$$

Now it is straightforward to derive the charged Rényi logarithmic negativity

$$\mathcal{E}_n(\mu) = \Delta_{n,\mu}^{(2)} \ln \frac{a\epsilon}{2(\epsilon^2 + t^2)} + \ln c_{n,\mu}. \quad (4.6)$$

The charged logarithmic negativity is obtained by taking replica limit  $n_e \rightarrow 1$

$$\mathcal{E}(\mu) = h(\mu) \ln \frac{a\epsilon}{2(\epsilon^2 + t^2)} + \tilde{c}, \quad h(\mu) = -\frac{1}{2} - \frac{\mu^2}{\pi^2} + \frac{2\mu}{\pi}, \quad (4.7)$$

where  $\tilde{c} = \lim_{n_e \rightarrow 1} \ln c_{n_e,\mu}$ . For  $t = 0$ , requiring

$$\mathcal{E}(\mu)|_{t=0} = h(\mu) \ln \frac{a}{2\epsilon} + \tilde{c} = 0, \quad (4.8)$$

based on which, it is enough to fix the factor  $\tilde{c}$ , we have

$$\mathcal{E}(\mu) = h(\mu) \ln \frac{\epsilon^2}{\epsilon^2 + t^2}. \quad (4.9)$$

In the limit  $t \gg \epsilon$ , we get

$$\mathcal{E}(\mu) = -2h(\mu) \ln \frac{t}{\epsilon}, \quad (4.10)$$

when  $\mu = 0$ , we have

$$\mathcal{E}(\mu = 0) = \ln \frac{t}{\epsilon}, \quad (4.11)$$

which is agree with the result obtained in Ref. [37]. For  $n = 1$ , the calculations are similar to the limit  $n_e \rightarrow 1$ , we end with

$$\mathcal{E}_1(\mu) = h_1(2\mu) \ln \frac{\epsilon^2}{\epsilon^2 + t^2}, \quad h_1(\mu) = -\frac{\mu^2}{4\pi^2} + \frac{\mu}{2\pi}. \quad (4.12)$$

### 4.1.2 Symmetric finite intervals

As shown in Fig.3, we consider the case of symmetric finite intervals with  $l_1 = l_2 = l$ , namely,  $A_1 \in [-l, 0]$  and  $A_2 \in (0, l]$ . In this case, by studying the three-point function in Eq. (3.6), quench dynamics of the charged Rényi negativity between two adjacent intervals can be obtained.  $\mathcal{F}(\{\eta_{j,k}\})$  is just a constant in the limits  $\eta_{i,j} \rightarrow 0, 1$ , or  $\infty$ . For symmetric intervals, it has been found that one always has  $\eta_{ij} = 1$  or  $0$  for the cases  $t \ll l$ ,  $t = l + 0^-$  and  $t > l$  [37]. Thus our results are universal for the above three cases. By neglecting various nonuniversal terms and using Eqs. (3.7), (3.9) and (3.10), we have

$$\mathcal{E}(\mu) = \begin{cases} h(\mu) \ln \frac{\epsilon^2}{\epsilon^2+t^2} + h(\mu) \ln \frac{l+t}{l-t} + 2h_1(\mu) \ln \frac{1}{2l}, & t < l \\ h(\mu) \ln \frac{\epsilon^2}{\epsilon^2+t^2} + h(\mu) \ln \frac{4t^2}{\epsilon l} + h_1(\mu) \ln \frac{(t-l)^2}{l^2[4(t-l)^2+4t^2\epsilon^2]}, & t > l \end{cases} \quad (4.13)$$

In the limit  $l, t \gg \epsilon$ , by subtracting the charged logarithmic negativity at  $t = 0$ , we end with

$$\mathcal{E}(\mu) = \begin{cases} h(\mu) \ln \frac{\epsilon^2(l+t)}{(\epsilon^2+t^2)(l-t)}, & t < l \\ h(\mu) \ln \frac{4\epsilon}{l}, & t > l \end{cases} \quad (4.14)$$

In the limit  $t \ll l$ , we get

$$\mathcal{E}(\mu) = h(\mu) \ln \frac{\epsilon^2}{\epsilon^2 + t^2}, \quad (4.15)$$

which is the same as Eq. (4.9). For  $t \leq l$ , our results are not accurate, because we neglect the nonuniversal functions  $\mathcal{F}(\{\eta_{j,k}\})$  which may not be constants. Thus we may not obtain the correct scaling behavior. For  $t > l$ , we can compute the ground-state value of  $\mathcal{E}(\mu)$  as

$$\mathcal{E}_G(\mu) = -h(\mu) \ln \frac{l}{4\epsilon}, \quad (4.16)$$

which is consistent with the result in Ref. [37].

### 4.1.3 Asymmetric finite intervals

We consider the case of asymmetric finite intervals with  $A_1 \in [-l_1, 0]$  and  $A_2 \in (0, l_2]$ . Without loss of generality, we assume  $l_1 < l_2$ . It has been found that one always has  $\eta_{ij} = 1$  or  $0$  for the cases  $t \ll l_1$ ,  $t = l_2 + 0^-$  and  $t > l_2$  [37]. Our results are universal in these cases. By neglecting the nonuniversal terms, the charged logarithmic negativity can be written as

$$\mathcal{E}(\mu) = \frac{h(\mu)}{2} \ln \left( \frac{\eta_{1,3}}{\eta_{1,2}\eta_{2,3}} \right). \quad (4.17)$$

In the limit  $l, t \gg \epsilon$ , we have

$$\mathcal{E}(\mu) = \begin{cases} \frac{h(\mu)}{2} \ln \frac{\epsilon^4(l_1+t)(l_2+t)}{t^4(l_1-t)(l_2-t)}, & t < l_1 \\ \frac{h(\mu)}{2} \ln \frac{4\epsilon^2(l_1+l_2)(l^2-l_1^2)}{(l_2-l_1)l_1^2t^2}, & l_1 < t < l_2 \\ h(\mu) \ln \frac{2\epsilon(l_1+l_2)}{l_1l_2}, & t > l_2 \end{cases} \quad (4.18)$$

In the limit  $l_1 = l_2$ , our result in Eq. (4.14) is reproduced. For  $t \leq l_2$ , similar to the symmetric case, our results are not accurate, because we neglected the nonuniversal functions  $\mathcal{F}(\{\eta_{j,k}\})$

which may not be constants. Thus one has to calculate  $\mathcal{F}(\{\eta_{j,k}\})$  for different CFTs. For  $t > l$ , we obtain the ground-state value of the charged logarithmic negativity as

$$\mathcal{E}_G(\mu) = -h(\mu) \ln \frac{l_1 l_2}{2\epsilon(l_1 + l_2)}, \quad (4.19)$$

which is consistent with the result in Ref. [37].

## 4.2 Two disjoint intervals

### 4.2.1 Symmetric finite intervals

As shown in Fig.3, we consider the case of symmetric finite intervals with  $A_1 \in [-d-l, -d]$  and  $A_2 \in [d, d+l]$ . In this case, by studying the four-point function in Eq. (3.4), quench dynamics of the charged Rényi negativity between two disjoint symmetric intervals can be obtained. As explicitly calculated in Ref. [39],  $\mathcal{F}(\{\eta_{j,k}\})$  are simply a constant in the limit  $l/d \ll 1$ . The calculations are similar to the two adjacent symmetric finite intervals case. In the limit  $l, t \gg \epsilon$ , by neglecting various nonuniversal terms, using Eqs. (3.5), (3.9) and (3.10) and subtracting the charged logarithmic negativity at  $t = 0$ , we have

$$\mathcal{E}(\mu) = \begin{cases} 0 & t < d \\ h(\mu) \ln \frac{\epsilon d l (d+l+t)}{(2d+l)(d+l-t)(t^2-d^2)} & d < t < d+l \\ h(\mu) \ln \frac{4d(d+l)}{(2d+l)^2} & t > d+l \end{cases} \quad (4.20)$$

### 4.2.2 Asymmetric finite intervals

In this case, we consider the case of asymmetric finite intervals with  $A_1 \in [-d_1-l_1, d_1]$  and  $A_2 \in [d_2, d_2+l_2]$ . Without loss of generality, we assume  $l_1 = l_2 = l$  and  $d_1 < d_2 \leq d_1+l$ . By neglecting the nonuniversal terms, the charged logarithmic negativity can be written as

$$\mathcal{E}(\mu) = \frac{h(\mu)}{2} \ln \left( \frac{\eta_{1,4} \eta_{2,3}}{\eta_{1,3} \eta_{2,4}} \right). \quad (4.21)$$

In the limit  $l, t \gg \epsilon$ , we have

$$\mathcal{E}(\mu) = \begin{cases} 0 & t < d_1 \\ \frac{h(\mu)}{2} \ln \frac{(d_1+d_2)(d_2-t)(d_2+l+t)(d_2-d_1+l)}{(d_1+d_2+l)(d_2+l-t)(d_2+t)(d_2-d_1)} & d_1 < t < d_2 \\ \frac{h(\mu)}{2} \ln \frac{\epsilon^2 (d_1+d_2)^2 (d_1+l-d_2)(d_2+l-d_1)(d_1+l+t)(d_2+l+t)}{4(d_1+d_2+l)^2 (d_1+l-t)(d_2+l-t)(t^2-d_1^2)(t^2-d_2^2)} & d_2 < t < d_1+l \\ \frac{h(\mu)}{2} \ln \frac{[t^2-(d_1+l)^2](d_1+d_2)^2 (d_2+l-d_1)(d_1+d_2+2l)}{(d_2-d_1)(d_1+d_2+l)^3 (t^2-d_1^2)} & d_1+l < t < d_2+l \\ h(\mu) \ln \frac{(d_1+d_2)(d_1+d_2+2l)}{(d_1+d_2+l)^2} & t > d_2+l \end{cases} \quad (4.22)$$

when  $d_1 = d_2 = d$ , our result in Eq. (4.20) is reproduced.

## 5 Charge imbalance resolved negativity in local joining quench

In this section, we consider the symmetric cases. It is easy to derive the charged imbalance resolved negativity in the asymmetric cases. For simplicity, we introduce some notations

$$\begin{aligned}
f_1 &\equiv \ln \frac{\epsilon^2}{\epsilon^2 + t^2}. \\
f_2 &\equiv \ln \frac{\epsilon^2(l+t)}{(\epsilon^2 + t^2)(l-t)}. \\
f_3 &\equiv \ln \frac{4\epsilon}{l}. \\
f_4 &\equiv \ln \frac{\epsilon dl(d+l+t)}{(2d+l)(d+l-t)(t^2-d^2)}. \\
f_5 &\equiv \ln \frac{4d(d+l)}{(2d+l)^2}.
\end{aligned} \tag{5.1}$$

### 5.1 Two adjacent intervals

#### 5.1.1 Semi-infinite intervals

During this region, we have

$$\mathcal{E}(\mu) = f_1 h(\mu), \quad \mathcal{E}_1(\mu) = f_1 h_1(2\mu), \tag{5.2}$$

when  $\mu = 0$ , we obtain

$$\mathcal{E}(0) = f_1 h(0). \tag{5.3}$$

By using Eq. (3.19), after normalization, we find that the probability distribution is given by

$$p(q) = -\frac{1 + (-1)^q}{\pi^2 q^2 / f_1 + f_1}, \tag{5.4}$$

after Fourier transformation in Eq. (3.21), we have

$$\mathcal{Z}_{T_2}(q) = \frac{-2f_1}{e^{\frac{f_1}{2}} (\pi^2 q^2 + 4f_1^2)}, \tag{5.5}$$

thus the charge imbalance resolved negativity is obtained from Eq. (3.22)

$$\mathcal{N}(q) = \frac{\pi^2 q^2 + f_1^2}{e^{\frac{f_1}{2}} (\pi^2 q^2 + 4f_1^2) (1 + (-1)^q)} - \frac{1}{2}. \tag{5.6}$$

#### 5.1.2 Symmetric finite intervals

$t < l$

In this region, we have

$$\mathcal{E}(\mu) = f_2 h(\mu), \quad \mathcal{E}_1(\mu) = f_2 h_1(2\mu), \tag{5.7}$$

the probability distribution is

$$p(q) = -\frac{1 + (-1)^q}{\pi^2 q^2 / f_2 + f_2}. \quad (5.8)$$

After Fourier transformation, we find

$$\mathcal{Z}_{T_2}(q) = \frac{-2f_2}{e^{\frac{f_2}{2}} (\pi^2 q^2 + 4f_2^2)}, \quad (5.9)$$

thus the charge imbalance resolved negativity is

$$\mathcal{N}(q) = \frac{\pi^2 q^2 + f_2^2}{e^{\frac{f_2}{2}} (\pi^2 q^2 + 4f_2^2) (1 + (-1)^q)} - \frac{1}{2}. \quad (5.10)$$

**$t > l$**

In this region, we have

$$\mathcal{E}(\mu) = f_3 h(\mu), \quad \mathcal{E}_1(\mu) = f_3 h_1(2\mu), \quad (5.11)$$

the probability distribution can be computed similarly, the final result is

$$p(q) = -\frac{1 + (-1)^q}{\pi^2 q^2 / f_3 + f_3}. \quad (5.12)$$

After Fourier transformation, we find

$$\mathcal{Z}_{T_2}(q) = \frac{-2f_3}{e^{\frac{f_3}{2}} (\pi^2 q^2 + 4f_3^2)}. \quad (5.13)$$

Then the charge imbalance resolved negativity is

$$\mathcal{N}(q) = \frac{\pi^2 q^2 + f_3^2}{e^{\frac{f_3}{2}} (\pi^2 q^2 + 4f_3^2) (1 + (-1)^q)} - \frac{1}{2}. \quad (5.14)$$

## 5.2 Two disjoint symmetric finite intervals

**$t < d$**

At this early time stage, we have  $\mathcal{E}(\mu) = \mathcal{E}_1(\mu)$ , therefore

$$\mathcal{N}(q) = 0. \quad (5.15)$$

**$d < t < d + l$**

In this time region, we have

$$p(q) = -\frac{1 + (-1)^q}{\pi^2 q^2 / f_4 + f_4}, \quad (5.16)$$

$$\mathcal{Z}_{T_2}(q) = \frac{-2f_4}{e^{\frac{f_4}{2}} (\pi^2 q^2 + 4f_4^2)}. \quad (5.17)$$

The charge imbalance resolved negativity is

$$\mathcal{N}(q) = \frac{\pi^2 q^2 + f_4^2}{e^{\frac{f_4}{2}} (\pi^2 q^2 + 4f_4^2) (1 + (-1)^q)} - \frac{1}{2}. \quad (5.18)$$

$t > d + l$

In this time region, we have

$$p(q) = -\frac{1 + (-1)^q}{\pi^2 q^2 / f_5 + f_5}, \quad (5.19)$$

$$\mathcal{Z}_{T_2}(q) = \frac{-2f_5}{e^{\frac{f_5}{2}} (\pi^2 q^2 + 4f_5^2)}. \quad (5.20)$$

The charge imbalance resolved negativity is

$$\mathcal{N}(q) = \frac{\pi^2 q^2 + f_5^2}{e^{\frac{f_5}{2}} (\pi^2 q^2 + 4f_5^2) (1 + (-1)^q)} - \frac{1}{2}. \quad (5.21)$$

### 5.3 Total negativity

To check our results, we should recover the total negativity from the charge imbalance resolved negativity. Using the following formula

$$\begin{aligned} \sum_{q=-\infty}^{+\infty} p(q) &= -\sum_{q=-\infty}^{+\infty} \frac{f}{\pi^2 q^2 + f^2} = -\coth(f) \xrightarrow{f \rightarrow -\infty} 1, \\ \sum_{q=-\infty}^{+\infty} p(q) \mathcal{N}(q) &= \frac{e^{-\frac{f}{2}} - 1}{2} = \frac{e^{\mathcal{E}(\mu=0)} - 1}{2} = \mathcal{N}, \end{aligned} \quad (5.22)$$

where  $\mathcal{E}(\mu = 0)$  is the total negativity given in Eq. (5.3), one could check our predictions. Indeed we have recovered the known quench dynamics of the total negativity from the charge imbalance resolved ones, confirming our results.

## 6 Numerical test

In this section, we first review the numerical approach to the charged logarithmic negativity after local joining quench (see [34,37,40] for more details). Then we compare the CFT predictions with the numerical results.

### 6.1 Numerical approach

To check our CFT predictions obtained in the previous sections, we will consider the time evolution of the logarithmic negativity after local joining quench in a complex harmonic chain which is the lattice version of our complex Klein-Gordon field. The Hamiltonian of the real harmonic chain is

$$H_{RHC} = \sum_{j=1}^{L-1} \left( \frac{1}{2M} p_j^2 + \frac{M\omega^2}{2} q_j^2 + \frac{K}{2} (q_{j+1} - q_j)^2 \right), \quad (6.1)$$

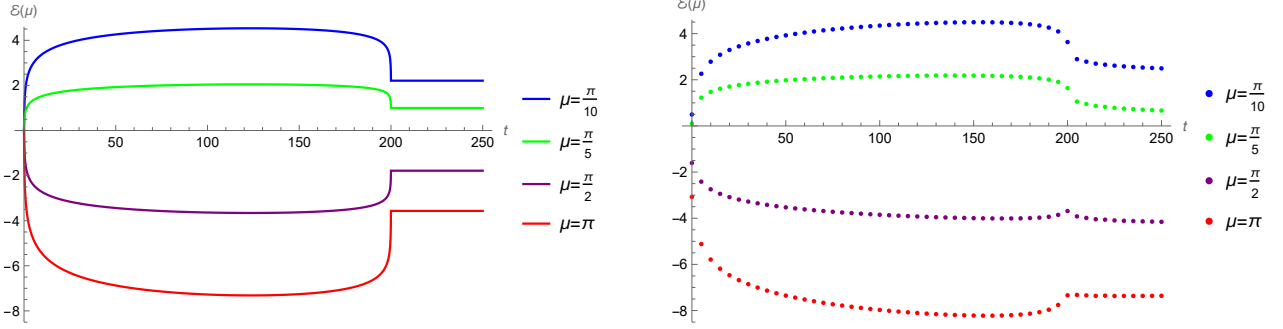


Figure 4: The charged logarithmic negativity  $\mathcal{E}(\mu)$  for two symmetric adjacent finite intervals as a function of time  $t$  for  $\mu = \frac{\pi}{10}, \frac{\pi}{5}, \frac{\pi}{2}, \pi$ , respectively. Here we choose  $L = 500, l = 200$  and  $\epsilon = 0.05$ . Left panel: CFT predictions. Right panel: numerical results in the complex harmonic chain.

where the Dirichlet boundary condition  $q_0 = q_L = p_0 = p_L = 0$  are imposed and variables  $p_j$  and  $q_j$  satisfy standard bosonic commutation relations  $[q_i, q_j] = [p_i, p_j] = 0$  and  $[q_i, p_j] = i\delta_{ij}$ .  $L$  is the number of sites of the chain,  $M$  is the mass scale, and  $K$  is the nearest-neighbor coupling constant. The complex harmonic chain is equivalent to two decoupled real harmonic chains. In terms of the variables  $q^{(1)}, p^{(1)}$  and  $q^{(2)}, p^{(2)}$ , the Hamiltonian becomes

$$H_{CHC}(p^{(1)} + ip^{(2)}, q^{(1)} + iq^{(2)}) = H_{RHC}(p^{(1)}, q^{(1)}) + H_{RHC}(p^{(2)}, q^{(2)}). \quad (6.2)$$

For the Dirichlet boundary condition, the Fourier sine transform of the canonical variables are

$$p_j = \sum_{k=1}^{L-1} \tilde{p}_k \sqrt{\frac{2}{L}} \sin\left(\frac{\pi kn}{L}\right), \quad \tilde{p}_k = \sum_{j=1}^{L-1} p_j \sqrt{\frac{2}{L}} \sin\left(\frac{\pi kn}{L}\right), \quad (6.3)$$

where  $j, k = 1, \dots, L-1$ . For  $q_j$ , the Fourier sine transformation is defined similarly. In the momentum space, the Hamiltonian is diagonal

$$H_{CHC} = \sum_{k=1}^{L-1} \left( \frac{1}{2M} \tilde{p}_k^2 + \frac{M\omega_k^2}{2} \tilde{q}_k^2 \right), \quad (6.4)$$

where the dispersion relation reads [37]

$$\omega_k = \sqrt{\omega_0^2 + \frac{4K}{M} \sin\left(\frac{\pi k}{2L}\right)^2} > \omega_0 \quad (6.5)$$

$\omega_0 = 0$  is well-defined while it is ill-defined in the periodic case. Now we introduce the creation and annihilation operators  $a_k, a_k^\dagger$  and  $b_k, b_k^\dagger$ , satisfying  $[a_k, a_{k'}^\dagger] = \delta_{kk'}$  and  $[b_k, b_{k'}^\dagger] = \delta_{kk'}$ . Then the Hamiltonian in Eq. (6.4) becomes

$$H_{CHC} = \sum_{k=1}^{L-1} \omega_k (a_k^\dagger a_k + b_k^\dagger b_k) \quad (6.6)$$

Next, we use the correlation matrix techniques to obtain the charged logarithmic negativity. The covariance matrix is constructed from two-point correlators of the real harmonic chain

$$\Gamma_{n,m} = \text{Re} \begin{pmatrix} \mathbb{Q}_{n,m} & \mathbb{M}_{n,m} \\ \mathbb{M}_{n,m}^\dagger & \mathbb{P}_{n,m} \end{pmatrix} \quad (6.7)$$

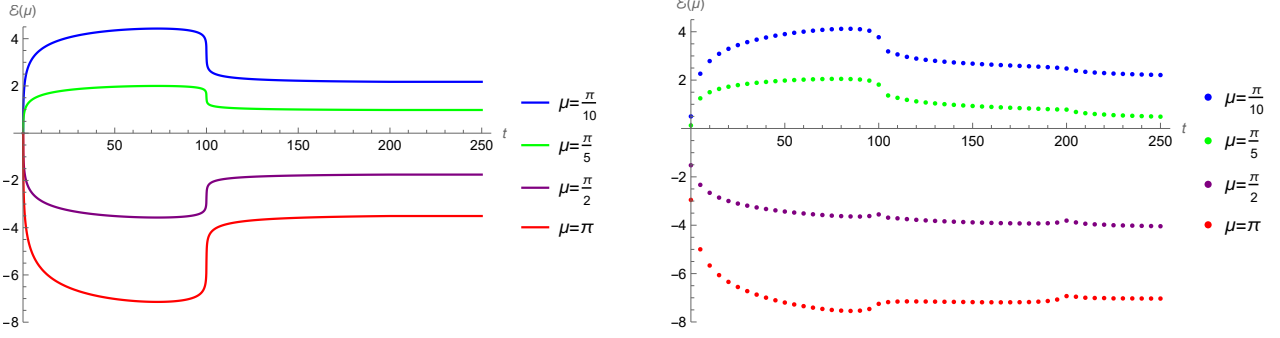


Figure 5: The charged logarithmic negativity  $\mathcal{E}(\mu)$  for two asymmetric adjacent finite intervals as a function of time  $t$  for  $\mu = \frac{\pi}{10}, \frac{\pi}{5}, \frac{\pi}{2}, \pi$ , respectively. Here we choose  $L=500$ ,  $l_1=100$ ,  $l_2=200$  and  $\epsilon = 0.03$ . Left panel: CFT predictions. Right panel: numerical results in the complex harmonic chain.

where

$$\begin{aligned}
\mathbb{Q}_{n,m} &\equiv \langle 0 | q_n q_m | 0 \rangle = \frac{1}{L} \sum_{k=1}^{L-1} \frac{1}{M \omega_k} \sin\left(\frac{\pi k n}{L}\right) \sin\left(\frac{\pi k m}{L}\right) \\
\mathbb{P}_{n,m} &\equiv \langle 0 | p_n p_m | 0 \rangle = \frac{1}{L} \sum_{k=1}^{L-1} M \omega_k \sin\left(\frac{\pi k n}{L}\right) \sin\left(\frac{\pi k m}{L}\right) \\
\mathbb{M}_{n,m} &\equiv \langle 0 | q_n p_m | 0 \rangle = \frac{i}{2} \delta_{nm}
\end{aligned} \tag{6.8}$$

with  $n, m = 1, \dots, L$ . Using the Heisenberg equation of motion,  $\dot{\tilde{q}}_k(t) = \frac{1}{M} \tilde{p}_k(t)$  and  $\dot{\tilde{p}}_k(t) = -M \omega_k^2 \tilde{q}_k(t)$ , we have

$$\begin{aligned}
\tilde{q}_k(t) &= \frac{1}{\sqrt{M}} (\cos \omega_k t \tilde{q}_k(0) + \omega_k^{-1} \sin \omega_k t \tilde{p}_k(0)), \\
\tilde{p}_k(t) &= \sqrt{M} (-\omega_k \sin \omega_k t \tilde{q}_k(0) + \cos \omega_k t \tilde{p}_k(0)).
\end{aligned} \tag{6.9}$$

The time-dependent canonical variables in the real space are

$$\begin{aligned}
q_j(t) &= \frac{1}{\sqrt{M}} \sum_{k,m} \phi_k^*(n) \phi_k(m) \times (\cos \omega_k t q_m(0) + \omega_k^{-1} \sin \omega_k t p_m(0)) \\
p_j(t) &= \sqrt{M} \sum_{k,m} \phi_k^*(n) \phi_k(m) \times (-\omega_k \sin \omega_k t q_m(0) + \cos \omega_k t p_m(0))
\end{aligned} \tag{6.10}$$

where

$$\phi_k(m) = \sqrt{\frac{2}{L}} \sin\left(\frac{\pi k m}{L}\right), \tag{6.11}$$

the time evolution of the covariance matrix is

$$\Gamma(t) = S(t) \Gamma(0) S(t)^T, \tag{6.12}$$



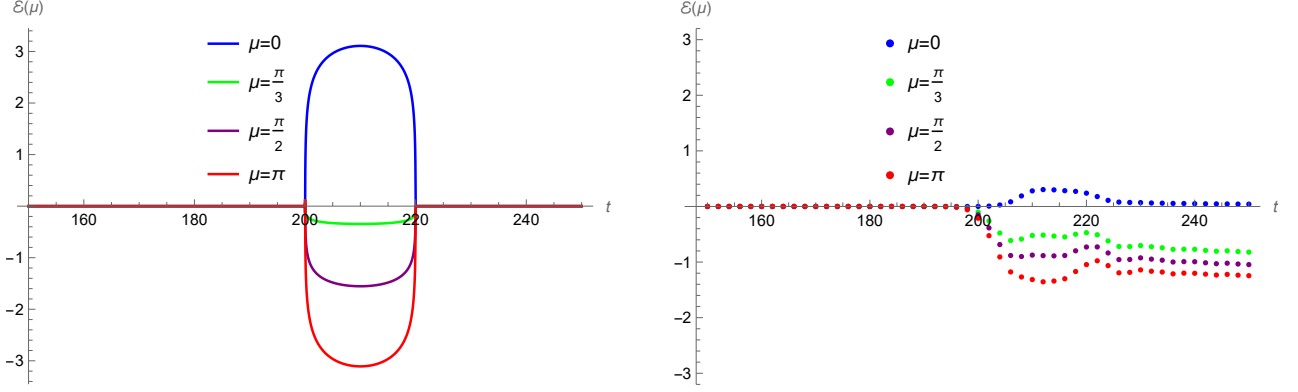


Figure 6: The charged logarithmic negativity  $\mathcal{E}(\mu)$  for two disjoint symmetric intervals as a function of time  $t$  for  $\mu = 0, \frac{\pi}{3}, \frac{\pi}{2}, \pi$ , respectively. Here we choose  $L = 500, l = 20, d = 200$  and  $\epsilon = 0.02$ . Left panel: CFT predictions. Right panel: numerical results in the complex harmonic chain.

where the evolution matrix is

$$\begin{aligned}
S_{n,m}(t) &= \sum_k \phi_k^*(n) \phi_k(m) \begin{pmatrix} \frac{1}{\sqrt{M}} \cos \omega_k t & \frac{1}{\sqrt{M}} \omega_k^{-1} \sin \omega_k t \\ -\sqrt{M} \omega_k \sin \omega_k t & \sqrt{M} \cos \omega_k t \end{pmatrix} \\
&= \sum_k \frac{2}{L} \sin \frac{\pi k n}{L} \sin \frac{\pi k m}{L} \begin{pmatrix} \frac{1}{\sqrt{M}} \cos \omega_k t & \frac{1}{\sqrt{M}} \omega_k^{-1} \sin \omega_k t \\ -\sqrt{M} \omega_k \sin \omega_k t & \sqrt{M} \cos \omega_k t \end{pmatrix}.
\end{aligned} \tag{6.13}$$

We first consider time evolution of covariance matrix  $\Gamma_A(t)$  and symplectic matrix  $J_A$  associated with the subsystem  $A$

$$\Gamma_A(t) = \begin{pmatrix} \mathbb{Q}_A(t) & \mathbb{R}_A(t) \\ \mathbb{R}_A(t)^\top & \mathbb{P}_A(t) \end{pmatrix}, \quad J_A = \begin{pmatrix} \mathbb{O}_l & \mathbb{I}_l \\ -\mathbb{I}_l & \mathbb{O}_l \end{pmatrix}, \tag{6.14}$$

where  $\mathbb{O}_l$  is zero matrix and  $\mathbb{I}_l$  is identity matrix. The spectrum of  $iJ_A\Gamma_A(t)$  denoted by  $\{\pm\lambda_1(t), \dots, \pm\lambda_l(t)\}$ . For the complex harmonic chain, the charged Rényi negativity factorizes as

$$N_n(\mu) = \text{Tr}[(\rho_A^{T_2})^n e^{i\mu \mathcal{Q}_A^a}] \times \text{Tr}[(\rho_A^{T_2})^n e^{-i\mu \mathcal{Q}_A^b}]. \tag{6.15}$$

We introduce the Fock space basis  $|\mathbf{n}\rangle \equiv \otimes_{j=1}^l |n_j\rangle$ , defined by products of eigenstates of the number operator in the subsystem  $A$ , the reduced density matrix of the subsystem  $A$  can be written as

$$\rho_A(t) = \sum_{\mathbf{n}} \prod_{j=1}^l \frac{1}{\lambda_j(t) + 1/2} \left( \frac{\lambda_j(t) - 1/2}{\lambda_j(t) + 1/2} \right)^{n_j} |\mathbf{n}\rangle \langle \mathbf{n}|. \tag{6.16}$$

In the Fock basis  $\{|\mathbf{n}\rangle\}$ ,  $Q_2^{T_2} = Q_2$  and the operator  $\mathcal{Q}_A = Q_1 - Q_2^{T_2} = Q_1 - Q_2$  becomes exactly the charge imbalance operator. We consider the partial transposition of  $\Gamma_A(t)$  with respect to  $A_2$

$$\Gamma_A^{T_2}(t) = \begin{pmatrix} \mathbb{I}_l & \mathbb{O}_l \\ \mathbb{O}_l & \mathbb{R}_{A_2} \end{pmatrix} \Gamma_A(t) \begin{pmatrix} \mathbb{I}_l & \mathbb{O}_l \\ \mathbb{O}_l & \mathbb{R}_{A_2} \end{pmatrix}, \tag{6.17}$$

where  $\mathbb{R}_{A_2}$  is the  $l_2 \times l_2$  diagonal matrix with elements  $(\mathbb{R}_{A_2})_{nm} = (-1)^{\delta_{n \in A_2}} \delta_{nm}$ .

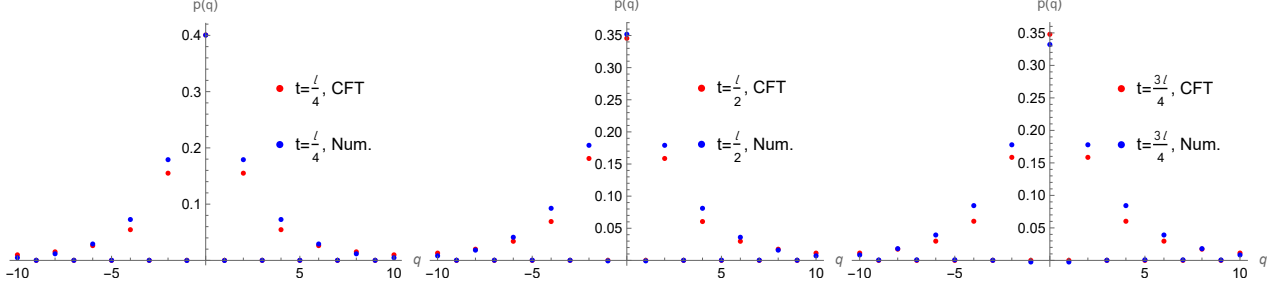


Figure 7: The probability  $p(q)$  for two adjacent symmetric finite intervals as a function of  $q$  for  $t = \frac{l}{4}, \frac{l}{2}, \frac{3l}{4}$ , respectively. Here we choose  $L = 500, l = 200$  and  $\epsilon = 3.2$ . Red dots: CFT predictions. Blue dots: numerical results in the complex harmonic chain.

We denote the eigenvalues of  $iJ_A\Gamma_A(t)^{T_2}$  by  $\{\pm\sigma_1(t), \pm\sigma_2(t), \dots, \pm\sigma_l(t)\}$ , the charged Rényi logarithmic negativity reads [34]

$$\mathcal{E}_n(\mu) = -2 \sum_{j=1}^{l_A} \log \left| \left( \sigma_j(t) + \frac{1}{2} \right)^n - e^{i\mu} \left( \sigma_j(t) - \frac{1}{2} \right)^n \right|, \quad (6.18)$$

for  $n = 1$ , we have

$$\mathcal{E}_1(\mu) = -2 \sum_{j=1}^{l_A} \log \left| \left( \sigma_j(t) + \frac{1}{2} \right) - e^{i\mu} \left( \sigma_j(t) - \frac{1}{2} \right) \right|. \quad (6.19)$$

The charged logarithmic negativity is given by

$$\mathcal{E}(\mu) = -2 \sum_{j=1}^{l_A} \log \left| \left| \sigma_j(t) + \frac{1}{2} \right| - e^{i\mu} \left| \sigma_j(t) - \frac{1}{2} \right| \right|. \quad (6.20)$$

At time  $t < 0$ , we consider two disconnected harmonic chains with equal number of sites  $L$  under the Dirichlet boundary condition with each harmonic chain initially prepared in its ground state. At time  $t = 0$ , two disconnected chains are joined together as one harmonic chain with the number of sites  $2L$  under the Dirichlet boundary condition. The evolution matrix in the situation is

$$S_{n,m}(t) = \frac{1}{L} \sum_{k=1}^{2L-1} \sin \frac{\pi kn}{2L} \sin \frac{\pi km}{2L} \begin{pmatrix} \frac{1}{\sqrt{M}} \cos \Omega_k t & \frac{1}{\sqrt{M}} \Omega_k^{-1} \sin \Omega_k t \\ -\sqrt{M} \Omega_k \sin \Omega_k t & \sqrt{M} \cos \Omega_k t \end{pmatrix}, \quad (6.21)$$

where  $\Omega_k = \sqrt{\omega_0^2 + \frac{4K}{M} \sin^2(\frac{\pi k}{4L})}$ . We calculate the charged logarithmic negativity by setting  $M = K = 1, \omega_0 = 0$ . We choose the total length of harmonic chain  $L = 500$ . The numerical data of quench dynamics of the charged logarithmic negativity are shown in Fig.4, Fig.5 and Fig.6. The numerical data of probability  $p(q)$  is shown in Fig.7. By comparing the CFT predictions with the numerical results obtained in the harmonic chain, we find that the main features agree well.

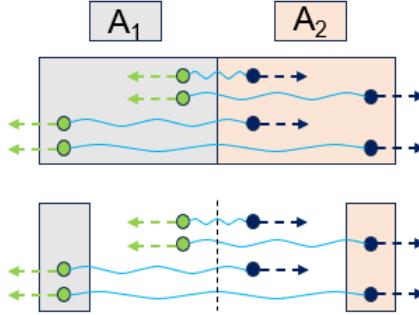


Figure 8: The classification of entangled pairs on charged logarithmic negativity  $\mathcal{E}(\mu)$  of two adjacent intervals and two disjoint intervals in the lattice model. For two adjacent intervals cases, all four kinds of entangled pairs contribute to the charged logarithmic negativity. For two disjoint intervals cases, however, only the fast-fast pairs can contribute to the charged logarithmic negativity near  $t \approx d$ .

## 6.2 Comparison between CFT predictions and numerical results

The quasi-particles picture of dynamics of entanglement negativity after local joining quench has been proposed in Ref. [37]. In CFT all the quasi-particles propagate at the speed of light  $v_c$  while in the lattice model is not. The dispersion relation in Eq. (6.5) can be written as

$$\omega_k = \sqrt{\omega^2 + 4 \sin\left(\frac{\pi k}{2L}\right)^2}, \quad (6.22)$$

from which it is easy to calculate the group velocities

$$v \equiv \frac{\partial \omega_k(p)}{\partial p} = \frac{\sin(p)}{\sqrt{\omega^2 + 4 \sin^2(p/2)}}, \quad p \equiv \frac{\pi k}{L}, \quad (6.23)$$

and to know that not all the quasi-particles have the same group velocities. In detail, the high-energy quasi-particles have the group velocities  $v < v_c$ . Following Ref. [37], as shown in Fig.8, we can divide the entangled pairs into four classes according to their group velocities  $(v_L, v_R)$ .

$$(v_L, v_R) \simeq \begin{cases} (-v, v), & \text{slow-slow pair} \\ (-v, v_c), & \text{slow-fast pair} \\ (-v_c, v), & \text{fast-slow pair} \\ (-v_c, v_c), & \text{fast-fast pair} \end{cases} \quad (6.24)$$

Although the main features of CFT predictions agree well with numerical results, we also observe that there are some disagreements between the two approaches. For two adjacent intervals cases, as shown in Fig.4 and Fig.5, the charged logarithmic negativity obtained in the harmonic chain arrives at the ground state gradually while calculated in CFT approach drops to the ground state value very suddenly. The reason is that there are only the contributions of fast-fast pairs in CFT, however, in the lattice model the slow-slow pairs still contribute to  $\mathcal{E}(\mu)$  even for  $t > l$  in the symmetric case and  $t > l_1$  in the asymmetric case. We also notice that the absolute value of  $\mathcal{E}(\mu)$  of CFT results are smaller than the numerical results for  $\mu = \frac{\pi}{2}, \pi$  during  $t > l$  in the symmetric case and  $t > l_1$  in the asymmetric case. The reason is that we have

neglected the nonuniversal functions  $\mathcal{F}(\{\eta_{j,k}\})$  in CFT. For two disjoint intervals case, as shown in Fig.6, the first disagreement is that the concrete values of the charged logarithmic negativity between CFT results and numerical results, namely, the numerical results are much smaller than the CFT results. By using the quasi-particles picture in Fig.8 again, we can explain this phenomenon. For two adjacent intervals, all four kinds of entangled pairs contribute to the charged logarithmic negativity. For two disjoint intervals case, however, only the fast-fast pairs can contribute to the charged logarithmic negativity during  $d < t < d+l$  in the symmetric case, and the other three kinds of entangled pairs do not make any contribution at all. Thus the CFT results are much larger than the numerical results for disjoint case. When  $\mu = 0$ , our case are similar to the case in Ref. [37], we find that the dynamics behaviors of negativity between them agree well, however, for  $\mu \neq 0$ , there is disagreement during  $t > d+l$ : The absolute value of  $\mathcal{E}(\mu)$  of CFT results are smaller than the numerical results, which is due to the fact that we have neglected the nonuniversal functions  $\mathcal{F}(\{\eta_{j,k}\})$  in CFT.

## 7 Conclusion

In this paper, we studied the dynamics of the charge imbalance resolved entanglement negativity after local joining quench. Firstly, we considered the local joining quench, in which the entangled pairs are generated at the joining point, then they propagate freely through the system. Secondly, we calculated the quench dynamics of charged logarithmic negativity, then by using Fourier transformation, we obtained the charge imbalance resolved negativity. Then the total negativity can be recovered from the charged imbalance resolved ones. We compare CFT predictions with the numerical results for quench dynamics of charged logarithmic negativity and probability. Finally, we explained the phenomenon based on the quasi-particle picture.

It will be an interesting problem to see how our results are changed in finite temperatures in the same quench protocol discussed in this paper. More interestingly, one could consider the non-equilibrium evolution of charge resolved entanglement where two CFTs are initially prepared at different temperatures suddenly joined together. In this setting, a non-equilibrium steady state should exist at late times [41].

## Acknowledgments

This work was supported by the National Natural Science Foundation of China, Grant No. 12005081.

## References

- [1] P. Calabrese and J. L. Cardy, “Entanglement entropy and quantum field theory,” *J. Stat. Mech.* **0406**, P06002 (2004) doi:10.1088/1742-5468/2004/06/P06002 [arXiv:hep-th/0405152 [hep-th]].
- [2] P. Calabrese and J. Cardy, “Entanglement entropy and conformal field theory,” *J. Phys. A* **42**, 504005 (2009) doi:10.1088/1751-8113/42/50/504005 [arXiv:0905.4013 [cond-mat.stat-mech]].

- [3] L. Amico, R. Fazio, A. Osterloh and V. Vedral, “Entanglement in many-body systems,” *Rev. Mod. Phys.* **80**, 517-576 (2008) doi:10.1103/RevModPhys.80.517 [arXiv:quant-ph/0703044 [quant-ph]].
- [4] P. Calabrese, J. Cardy and E. Tonni, “Finite temperature entanglement negativity in conformal field theory,” *J. Phys. A* **48**, no.1, 015006 (2015) doi:10.1088/1751-8113/48/1/015006 [arXiv:1408.3043 [cond-mat.stat-mech]].
- [5] A. Coser, E. Tonni and P. Calabrese, “Towards the entanglement negativity of two disjoint intervals for a one dimensional free fermion,” *J. Stat. Mech.* **1603**, no.3, 033116 (2016) doi:10.1088/1742-5468/2016/03/033116 [arXiv:1508.00811 [cond-mat.stat-mech]].
- [6] T. Nishioka, S. Ryu and T. Takayanagi, “Holographic Entanglement Entropy: An Overview,” *J. Phys. A* **42**, 504008 (2009) doi:10.1088/1751-8113/42/50/504008 [arXiv:0905.0932 [hep-th]].
- [7] S. N. Solodukhin, “Entanglement entropy of black holes,” *Living Rev. Rel.* **14**, 8 (2011) doi:10.12942/lrr-2011-8 [arXiv:1104.3712 [hep-th]].
- [8] S. Ryu and T. Takayanagi, “Holographic derivation of entanglement entropy from AdS/CFT,” *Phys. Rev. Lett.* **96**, 181602 (2006) doi:10.1103/PhysRevLett.96.181602 [arXiv:hep-th/0603001 [hep-th]].
- [9] A. Faraji Astaneh and A. E. Mosaffa, “Holographic Entanglement Entropy for Excited States in Two Dimensional CFT,” *JHEP* **03**, 135 (2013) doi:10.1007/JHEP03(2013)135 [arXiv:1301.1495 [hep-th]].
- [10] M. Nozaki, T. Numasawa, A. Prudenziati and T. Takayanagi, “Dynamics of Entanglement Entropy from Einstein Equation,” *Phys. Rev. D* **88**, no.2, 026012 (2013) doi:10.1103/PhysRevD.88.026012 [arXiv:1304.7100 [hep-th]].
- [11] K. K. Kim, O. K. Kwon, C. Park and H. Shin, “Holographic entanglement entropy of mass-deformed Aharony-Bergman-Jafferis-Maldacena theory,” *Phys. Rev. D* **90**, no.12, 126003 (2014) doi:10.1103/PhysRevD.90.126003 [arXiv:1407.6511 [hep-th]].
- [12] N. Kim and J. Hun Lee, “Time-evolution of the holographic entanglement entropy and metric perturbations,” *J. Korean Phys. Soc.* **69**, no.4, 623-631 (2016) doi:10.3938/jkps.69.623 [arXiv:1512.02816 [hep-th]].
- [13] J. Tsujimura and Y. Nambu, “Holographic entanglement entropy of two disjoint intervals in  $AdS_3/CFT_2$ ,” [arXiv:2106.00015 [hep-th]].
- [14] P. Chaturvedi, V. Malvimat and G. Sengupta, “Holographic Quantum Entanglement Negativity,” *JHEP* **05**, 172 (2018) doi:10.1007/JHEP05(2018)172 [arXiv:1609.06609 [hep-th]].
- [15] P. Jain, V. Malvimat, S. Mondal and G. Sengupta, “Covariant holographic entanglement negativity for adjacent subsystems in  $AdS_3/CFT_2$ ,” *Nucl. Phys. B* **945**, 114683 (2019) doi:10.1016/j.nuclphysb.2019.114683 [arXiv:1710.06138 [hep-th]].
- [16] P. Jain, V. Malvimat, S. Mondal and G. Sengupta, “Holographic entanglement negativity conjecture for adjacent intervals in  $AdS_3/CFT_2$ ,” *Phys. Lett. B* **793**, 104-109 (2019) doi:10.1016/j.physletb.2019.04.037 [arXiv:1707.08293 [hep-th]].

- [17] V. Malvimat, S. Mondal, B. Paul and G. Sengupta, “Holographic entanglement negativity for disjoint intervals in  $AdS_3/CFT_2$ ,” *Eur. Phys. J. C* **79**, no.3, 191 (2019) doi:10.1140/epjc/s10052-019-6693-8 [arXiv:1810.08015 [hep-th]].
- [18] M. Afrasiar, J. Kumar Basak, V. Raj and G. Sengupta, “Holographic Entanglement Negativity for Disjoint Subsystems in Conformal Field Theories with a Conserved Charge,” [arXiv:2106.14918 [hep-th]].
- [19] G. Vidal and R. F. Werner, “Computable measure of entanglement,” *Phys. Rev. A* **65**, 032314 (2002) doi:10.1103/PhysRevA.65.032314 [arXiv:quant-ph/0102117 [quant-ph]].
- [20] P. Calabrese and J. Cardy, “Quantum Quenches in Extended Systems,” *J. Stat. Mech.* **0706**, P06008 (2007) doi:10.1088/1742-5468/2007/06/P06008 [arXiv:0704.1880 [cond-mat.stat-mech]].
- [21] P. Calabrese and J. L. Cardy, “Time-dependence of correlation functions following a quantum quench,” *Phys. Rev. Lett.* **96**, 136801 (2006) doi:10.1103/PhysRevLett.96.136801 [arXiv:cond-mat/0601225 [cond-mat]].
- [22] P. Calabrese and J. Cardy, “Entanglement and correlation functions following a local quench: a conformal field theory approach,” *J. Stat. Mech.* **0710**, no.10, P10004 (2007) doi:10.1088/1742-5468/2007/10/P10004 [arXiv:0708.3750 [cond-mat.stat-mech]].
- [23] M. Nozaki, T. Numasawa and T. Takayanagi, “Holographic Local Quenches and Entanglement Density,” *JHEP* **05**, 080 (2013) doi:10.1007/JHEP05(2013)080 [arXiv:1302.5703 [hep-th]].
- [24] A. Jahn and T. Takayanagi, “Holographic entanglement entropy of local quenches in  $AdS_4/CFT_3$ : a finite-element approach,” *J. Phys. A* **51**, no.1, 015401 (2018) doi:10.1088/1751-8121/aa8afa [arXiv:1705.04705 [hep-th]].
- [25] P. Caputa, G. Mandal and R. Sinha, “Dynamical entanglement entropy with angular momentum and  $U(1)$  charge,” *JHEP* **11**, 052 (2013) doi:10.1007/JHEP11(2013)052 [arXiv:1306.4974 [hep-th]].
- [26] S. Matsuura, X. Wen, L. Y. Hung and S. Ryu, “Charged Topological Entanglement Entropy,” *Phys. Rev. B* **93**, no.19, 195113 (2016) doi:10.1103/PhysRevB.93.195113 [arXiv:1601.03751 [cond-mat.str-el]].
- [27] M. Goldstein and E. Sela, “Symmetry-resolved entanglement in many-body systems,” *Phys. Rev. Lett.* **120**, no.20, 200602 (2018) doi:10.1103/PhysRevLett.120.200602 [arXiv:1711.09418 [cond-mat.stat-mech]].
- [28] E. Cornfeld, M. Goldstein and E. Sela, “Imbalance entanglement: Symmetry decomposition of negativity,” *Phys. Rev. A* **98**, no.3, 032302 (2018) doi:10.1103/PhysRevA.98.032302 [arXiv:1804.00632 [cond-mat.stat-mech]].
- [29] S. Murciano, G. Di Giulio and P. Calabrese, “Entanglement and symmetry resolution in two dimensional free quantum field theories,” *JHEP* **08**, 073 (2020) doi:10.1007/JHEP08(2020)073 [arXiv:2006.09069 [hep-th]].

- [30] S. Murciano, R. Bonsignori and P. Calabrese, “Symmetry decomposition of negativity of massless free fermions,” *SciPost Phys.* **10**, no.5, 111 (2021) doi:10.21468/SciPostPhys.10.5.111 [arXiv:2102.10054 [cond-mat.stat-mech]].
- [31] H. Gaur and U. A. Yajnik, “Charge imbalance resolved Rényi negativity for free compact boson: Two disjoint interval case,” *JHEP* **02**, 118 (2023) doi:10.1007/JHEP02(2023)118 [arXiv:2210.06743 [hep-th]].
- [32] P. Jain, V. Malvimat, S. Mondal and G. Sengupta, “Holographic Entanglement Negativity for Conformal Field Theories with a Conserved Charge,” *Eur. Phys. J. C* **78**, no.11, 908 (2018) doi:10.1140/epjc/s10052-018-6383-y [arXiv:1804.09078 [hep-th]].
- [33] G. Perez, R. Bonsignori and P. Calabrese, “Dynamics of charge-imbalance-resolved entanglement negativity after a quench in a free-fermion model,” *J. Stat. Mech.* **2205**, no.5, 053103 (2022) doi:10.1088/1742-5468/ac666c [arXiv:2202.05309 [cond-mat.stat-mech]].
- [34] H. H. Chen, “Dynamics of charge imbalance resolved negativity after a global quench in free scalar field theory,” *JHEP* **08**, 146 (2022) [erratum: *JHEP* **10**, 157 (2022)] doi:10.1007/JHEP08(2022)146 [arXiv:2205.09532 [hep-th]].
- [35] N. Feldman and M. Goldstein, “Dynamics of Charge-Resolved Entanglement after a Local Quench,” *Phys. Rev. B* **100**, no.23, 235146 (2019) doi:10.1103/PhysRevB.100.235146 [arXiv:1905.10749 [cond-mat.stat-mech]].
- [36] M. Nozaki, T. Numasawa and T. Takayanagi, “Quantum Entanglement of Local Operators in Conformal Field Theories,” *Phys. Rev. Lett.* **112**, 111602 (2014) doi:10.1103/PhysRevLett.112.111602 [arXiv:1401.0539 [hep-th]].
- [37] X. Wen, P. Y. Chang and S. Ryu, “Entanglement negativity after a local quantum quench in conformal field theories,” *Phys. Rev. B* **92**, no.7, 075109 (2015) doi:10.1103/PhysRevB.92.075109 [arXiv:1501.00568 [cond-mat.stat-mech]].
- [38] H. H. Chen, “Charged Rényi negativity of massless free bosons,” *JHEP* **02**, 117 (2022) doi:10.1007/JHEP02(2022)117 [arXiv:2111.11028 [hep-th]].
- [39] C. T. Asplund and A. Bernamonti, “Mutual information after a local quench in conformal field theory,” *Phys. Rev. D* **89**, no.6, 066015 (2014) doi:10.1103/PhysRevD.89.066015 [arXiv:1311.4173 [hep-th]].
- [40] P. Calabrese, J. Cardy and E. Tonni, “Entanglement negativity in extended systems: A field theoretical approach,” *J. Stat. Mech.* **1302**, P02008 (2013) doi:10.1088/1742-5468/2013/02/P02008 [arXiv:1210.5359 [cond-mat.stat-mech]].
- [41] M. Hoogeveen and B. Doyon, “Entanglement negativity and entropy in non-equilibrium conformal field theory,” *Nucl. Phys. B* **898**, 78-112 (2015) doi:10.1016/j.nuclphysb.2015.06.021 [arXiv:1412.7568 [cond-mat.stat-mech]].